First-principles modeling of the magneto-optical response in inhomogeneous systems

Fabio Ricci,[1] Franco D'Orazio,[1,2] Alessandra Continenza,[1,2] Franco Lucari,[1,3] and Arthur J. Freeman[4]
[1]*Dipartimento di Fisica, Università di L'Aquila, I-67100 Coppito, L'Aquila, Italy*
[2]*Consorzio Nazionale Interuniversitario Scienze Fisiche della Materia (CNISM) at Dipartimento di Fisica, Università di L'Aquila, I-67100 Coppito, L'Aquila, Italy*
[3]*Consiglio Nazionale delle Ricerche-Istituto Nazionale di Fisica della Materia (CNR-INFM) at Dipartimento di Fisica, Università di L'Aquila, I-67100 Coppito, L'Aquila, Italy*
[4]*Department of Physics and Astronomy, Northwestern University, Evanston, Illinois 60208, USA*
(Received 10 April 2008; published 14 October 2008)

We develop an *ab initio* computational approach to calculate the magneto-optical Kerr effect spectra of layered and nanogranular compounds as a function of several structural and geometrical parameters: (i) composition, (ii) film thickness, and (iii) position, thickness, and number of the nonmagnetic interlayers. The case of nanoparticles in a matrix is treated within the effective-medium approximation and compared to a model (alternating composition layers approximation) that considers different compounds in a thin-film multilayered structure. The magneto-optical filter-amplifier effect of a nonmagnetic overlayer or interlayer and the dependence of the Kerr response on the specific sample composition suggest that our computational approach is a good starting point to build up structures with the desired magneto-optical characteristics and can be used to interpret experimental spectra to single out the microscopic structure and composition of the sample. The model is applied to the Mn-Ge binary system, considering both Mn_5Ge_3 as a film or in a nanoparticle arrangement and Mn_xGe_{1-x} diluted semiconductor as possible phases in pure form or intermixed with Ge.

DOI: 10.1103/PhysRevB.78.134411 PACS number(s): 71.15.−m, 78.20.Ls, 75.50.Tt, 75.50.Pp

I. INTRODUCTION

Magneto-optics is a physical phenomenon exploited to characterize magnetic materials. In particular, the magneto-optical (MO) Kerr effect (MOKE) is often used to determine the magnetic response of films and multilayers due to its surface sensitive nature. When dealing with multicomponent materials, the way different chemical compounds aggregate to form the final specimen structure greatly affects the actual MO response since it acts on both characters (magnetic and optical) of the phenomenon. Therefore, when using magneto-optics to probe layered or nanogranular materials, particular attention has to be paid to correctly interpret the results. A large variety of systems may be found where intermixing of different phases is required in order to take advantage of peculiar magnetic phenomena; a few examples are spin valves, magnetic recording, exchange bias, giant magnetoresistance, and spintronics. In this last field, which exploits the quantum spin states of electrons as well as their charge state, diluted magnetic semiconductors (DMS) have recently interested the scientific community due to their twofold semiconductor-magnetic behavior[1] and their highly spin-polarized currents. In particular, the discovery that Mn acts as a source of charge carriers and magnetic moments simultaneously, when doping III–V and group IV crystals, has increased interest in this direction. For example, the study of Mn-doped Ge DMS has gained a good deal of attention due to the linear dependence of the Curie temperature on Mn concentration.[2] However, both standard molecular-beam epitaxy (MBE) growth[3] and ion implantation[4–7] showed that Mn dilution competes with the formation of amorphous or crystal clusters. These aggregates have been unambiguously identified as principally Mn_5Ge_3.[5,8,9] Therefore, structural homogeneity is a crucial point also in the area of DMS and may influence the MO data. From the theoretical point of view, unfortunately, it is difficult to treat systems with highly inhomogeneous character. It is evident that in order to obtain reliable optical and magneto-optical properties from *ab initio* calculations, the sample's nanoscopic structure needs to be considered in detail.

The present work represents a step forward in this direction since it allows us to predict MO response of an inhomogeneous sample starting from *ab initio* calculations of the constituents' response in their bulk form. In the theoretical framework presented, the intermixed phases are accounted for within the theoretical MO treatment, using the effective-medium approximation (EMA) (Ref. 10) or the "alternating composition layers approximation" (ACLA), to describe nanogranular magnetic systems. The latter approximation, defined below, is implemented by building on the Zak model,[11,12] which is shown to satisfactorily describe multilayered structures. In this regard, we need to remark that in recent years a large effort has been made to gain a deep understanding of the magnetic properties of nanogranular films[13] due to their potential use in device applications. In particular, the modification of the magnetic properties as a function of grain size[14] and the interplay between the matrix and the material particle has interested the scientific community. Borcia *et al.*,[15] for example, observed a reasonable agreement between the MOKE experimental results obtained on Au/Co-Ag/Ag granular thin films grown by ultrahigh-vacuum (UHV) deposition, and simulations of the granular structure of the system. Clavero *et al.*[16] discussed the MO response of Co nanoparticles embedded in MgO, grown by a sputtering technique at different deposition temperatures, as a function of their size and concentration. They associate the changes in MO response with the decrease in the relaxation time of the electrons in the Co grains, induced by a reduction in the mean-free path due to the nanoparticle structure.

Menéndez *et al.*[17] studied the MOKE spectra of Fe nanoparticles in Al_2O_3 as a function of particle shape and size and obtained an acceptable agreement between theory and experiments. Ahn *et al.*[18] considered the optical properties of SiC whisker-Al_2O_3 obtained by applying high pressure on Al_2O_3 powders and SiC whiskers. The measured conductivities and the predictions obtained within the EMA limit of the Maxwell-Garnet theory (MGT) (Ref. 10) are in good agreement.

MOKE measurements and simulations have been carried out on multifilm systems as well. Vashuk *et al.*,[19] for example, measured $\{Co_{0.45}Fe_{0.45}Zr_{0.1}/a\text{-}Si\}_n$ and $\{Co_{0.45}Fe_{0.45}Zr_{0.1}/a\text{-}SiO_2\}_n$ multilayers and analyzed the MOKE spectra on the basis of EMA and macroscopic Fresnel magneto-optics.[20] They argued that the magnitude and form of the MO spectra depend on the magnetic and nonmagnetic layer thickness and the quantity of nonmagnetic material.

Here we examine the Mn-Ge binary compound, and we use it as a prototype system to develop a computational procedure to design engineered structures suitable for MO devices. We use *ab initio* MO calculations adapted to the structure of different samples, including their layered and nanogranular character. In Sec. II, we summarize the theoretical methods used to perform (i) *ab initio* simulations (Sec. II A), (ii) calculations of the MO response of multilayers (Sec. II B), and (iii) EMA to evaluate the optical conductivity of inhomogeneous media (Sec. II C). Section III shows our theoretical results based on different kinds of materials and structural geometry. Then in Sec. IV, we draw our conclusions.

II. THEORY

A. Density-functional theory and magneto-optics

MOKE is the change in polarization experienced by light when reflected by a magnetic sample. Linearly polarized light becomes elliptically polarized; the resulting ellipse has its major axis rotated by an angle θ_k (the Kerr rotation angle) with respect to the initial polarization direction, and the ratio between the minor and major axes is equal to ε_k (the Kerr ellipticity).[21]

Today, MOKE has become an important magnetic characterization tool in the field of magnetic thin films and multilayers since magneto-optics is the result of cooperative effects of spin-orbit coupling and exchange interaction in establishing the interband transitions involved. In fact, the MOKE spectrum in a particular geometry can be derived theoretically from the optical and MO coefficients, which are specific to each material. These coefficients are related to the conductivity tensor $\sigma(\omega)$, which can be obtained at any incoming photon energy on the basis of the material band structure. Therefore, this tensor can be computed from a first-principles approach based on density-functional theory (DFT). We recall for cubic structures and in polar geometry [i.e., when the magnetization is perpendicular to the reflecting surface taken in the (x,y) plane] that σ has the form,

$$\sigma = \begin{pmatrix} \sigma_{xx} & \sigma_{xy} & 0 \\ -\sigma_{xy} & \sigma_{xx} & 0 \\ 0 & 0 & \sigma_{zz} \end{pmatrix}, \quad (\vec{M} \parallel z). \tag{1}$$

The σ tensor is calculated within linear-response theory by solving self-consistently the Dirac-Kohn-Sham equations.[22] The Kubo formalism is used to write the conductivity matrix elements as follows:[23]

$$\sigma_{\lambda\lambda'}(\omega) = \frac{ie}{m^2\hbar V}\sum_{i,j}\frac{1}{\omega_{ij}}\left[\frac{\Pi_{ij}^{\lambda}\Pi_{ji}^{\lambda'}}{\omega-\omega_{ij}+\frac{i}{\tau}} - \frac{\Pi_{ij}^{\lambda}\Pi_{ji}^{\lambda'}}{\omega+\omega_{ij}+\frac{i}{\tau}}\right], \tag{2}$$

where the sum is taken between the occupied and unoccupied states (i and j, respectively), Π_{ij}^{λ} is the λth component ($\lambda=x,y,z$) of the dipole matrix calculated between the i and j states, τ is the interband relaxation time, and $\hbar\omega_{ij}$ are the transition energies.

In order to include intraband contributions, we add a phenomenological Drude term to the diagonal terms of the conductivity tensor as[24]

$$\sigma_D(\omega) = \frac{\omega_p^2}{4\pi(1-i\omega\tau_D)}. \tag{3}$$

Here, $\omega_p^2=\frac{4\pi e^2}{mV}\Sigma_{i\mathbf{k},\lambda}\delta(\varepsilon_{i\mathbf{k}}-E_F)|\Pi_{ii}^{\lambda}|^2$ is the plasma frequency, with E_F as the Fermi energy, and $\tau_D=\frac{m}{\rho ne^2}$ is the Drude relaxation time (where ρ is the dc electrical resistivity). The value of the plasma frequency depends on the electron density n of the material considered: for an insulator with $n \approx 10^{18}$ e/cm^3, $\hbar\omega_p \sim 1$ meV; for a metal with $n \approx 10^{22}$ e/cm^3, $\hbar\omega_p \sim 3.6$ eV. Therefore, intraband contributions are usually negligible for semiconductors and insulators.

In the calculations reported in Sec. III, we use accurate DFT methods, namely, the all-electron full-potential linearized augmented plane-wave (FLAPW) method,[24] within the local spin-density approximation (LSDA) to compute the conductivity tensor of Mn_5Ge_3 and DMS Mn_xGe_{1-x}. In the simulations of the former material, we used muffin-tin radii of 2.0 and 2.4 a.u. for Ge and Mn, respectively; wave functions and charge-density cutoffs were set at 3.2 and 7.0 a.u., respectively. For Mn_xGe_{1-x}, the muffin-tin radii were 2.1 and 2.3 a.u. for Ge and Mn, respectively; the charge-density cutoffs were 3.8 and 8.0 a.u., respectively. For both systems, $4\times4\times4$ **k**-points grid in the Brillouin zone were chosen according to the Monkhorst-Pack model.[25]

The values of ω_p for Mn-doped Ge (Ref. 26) and Mn_5Ge_3 (Ref. 27) were calculated from first principles on the basis of the band structure (in the same way shown in Ref. 28), and in accordance with these results, we take $\hbar\omega_p=1.8$ eV both for Mn_xGe_{1-x} and Mn_5Ge_3 compounds. Typical values of the Drude relaxation time in metals are in the range $0.01 < \hbar/\tau_D < 0.50$ eV. Since in our formalism $\hbar/\tau_D$ is a parameter, it is set at 0.45 eV in analogy with other published calculations.[28] Tests made on the effects of these quantities on the diagonal conductivity (σ_{xx}) show differences of a few percent in the low-energy range for both DMS Mn_xGe_{1-x} and Mn_5Ge_3, whereas, at high energy, the differences become

negligible. The corresponding MOKE spectra (not shown) maintain a similar behavior with appreciable differences limited to the low range of photon energies (below 1.0 eV for Mn_xGe_{1-x} and 0.5 eV for Mn_5Ge_3). For these reasons, all our calculations of the conductivity tensor (and then the MOKE spectra) include only the interband transitions with a relaxation time $\hbar/\tau=0.40$ eV [see Eq. (2)]—a typical value which accounts for experimental peak broadening and electron scattering with lattice defects, phonons, and magnons. Finally, the conductivity tensor for pure Ge was derived from optical data[29] due to the well-known difficulties with DFT-LSDA in obtaining a good description of the exited states in semiconductors and insulators.

B. Zak model

In order to calculate the MO effects (i.e., rotation and ellipticity for reflected and transmitted radiation) of geometrically complex structures such as films and multilayers, Zak *et al.*[11,12] developed a universal approach that treats both magnetic and nonmagnetic layers in a generalized way. This approach is based on the definition of two 4×4 matrices for each material present in the sample, regardless of their magnetic character: the *medium boundary* A and the *medium propagation* D matrices. The former matrix contains the boundary conditions for the radiation at the interface of a medium, i.e., the requirements for the continuity of the electric and magnetic-field components parallel to the surface; the latter defines the evolution of the same vectors when traveling through a medium. The model leads to a set of inhomogeneous linear equations for the optical and MO coefficients for each wave polarization (s or p) whose solution provides the response in all possible configurations. Within this model, a simple bulk magnetic material is represented as a system composed of two semi-infinite media (air-magnetic material) using the A matrix only. Multilayered samples require the presence of the D matrix for each layer with finite thickness and a medium boundary matrix A for each material, regardless of its thickness.

We can formalize the general problem of reflection as follows: we have a sequence of layers (each made of an arbitrary medium) and we want to compute the complex Kerr angle $\phi_k=\theta_k+i\varepsilon_k$. The electromagnetic radiation travels from the initial (semi-infinite) medium (i) and is transmitted through all layers, stacked along the z axis, before reaching the final (semi-infinite) substrate medium (f). The continuity conditions in this process are given by the so-called 4×4 M matrix,[11,12]

$$M = A_i^{-1}\left[\prod_{m=1}^{l}(A_m D_m A_m^{-1})\right]A_f \equiv \begin{pmatrix} G & H \\ I & J \end{pmatrix}, \tag{4}$$

where A_i and A_f are the medium boundary matrices for the initial and final media, respectively, A_m and D_m are the medium boundary and the propagation matrices, respectively, for the mth layer, l is the total number of layers, and G, I, H, and J are 2×2 properly defined block matrices of the 4×4 M matrix.

The elements of the M matrix contain all the information needed to describe any MO effect. In particular, knowledge of the G and I submatrices is enough to obtain the MO Fresnel reflection (r) or transmission (t) coefficients,

$$\begin{pmatrix} t_{ss} & t_{sp} \\ t_{ps} & t_{pp} \end{pmatrix} = G^{-1}, \tag{5}$$

$$\begin{pmatrix} r_{ss} & r_{sp} \\ r_{ps} & r_{pp} \end{pmatrix} = IG^{-1}. \tag{6}$$

The first subscript in each coefficient identifies the perpendicular (s) or parallel (p) component of the *outcoming* electric field with respect to the reflection plane; the second subscript indicates that the linear polarization of the *incoming* wave is either perpendicular (s) or parallel (p) to the reflection plane. The complex MO Kerr angle is, then, defined as[12]

$$\phi_s = \frac{r_{ps}}{r_{ss}} = \theta_s + i\varepsilon_s, \tag{7}$$

$$\phi_p = \frac{r_{sp}}{r_{pp}} = -\theta_p + i\varepsilon_p, \tag{8}$$

in terms of the rotation (θ) and ellipticity (ε). Using this formalism, we can calculate the Kerr response in all possible geometries: any polarization of the incident light, any magnetization direction, and any angle of incidence of light with respect to the sample surface can be considered on the same footing. Moreover, this theory treats bulk systems and/or film systems on the same basis, including the presence of nonmagnetic media as well.

C. Effective-medium approximation

In order to describe the optical and MO properties of nanogranular systems, it is essential to work out a theory that takes into account the composition inhomogeneities. This problem is faced by the Maxwell-Garnet theory, which assumes a randomly varying conductivity as a function of the spatial coordinates. Then, the self-consistent solution for the effective conductivity tensor $\bar{\sigma}_e$ of the entire medium is obtained by solving[10]

$$\langle \delta\bar{\sigma}(\bar{1} - \delta\bar{\sigma}\bar{\Gamma})^{-1}\rangle = 0. \tag{9}$$

Here, $\delta\bar{\sigma}=\bar{\sigma}_e-\bar{\sigma}(\mathbf{r})$, with $\bar{\sigma}(\mathbf{r})$ as the local conductivity tensor, the brackets denote a volume average, and $\bar{\Gamma}$ is a diagonal tensor whose elements depend self-consistently on the effective conductivity and on the demagnetization factors[30] of the material (i.e., on the shape of the grains). When the inhomogeneities consist of particles in an otherwise homogeneous matrix, we have that $\bar{\sigma}(\mathbf{r})=\bar{\sigma}_i$, with $i=p$ or h, for the portion of the volume occupied by particles or host matrix, respectively.

The EMA formalism can be applied to media composed of particles of all shapes and sizes embedded in a matrix under some assumptions.[16–18] In particular, the wavelength of the probing electromagnetic radiation must be much larger than the cluster size. Also, we suppose that $\bar{\sigma}_p$ and $\bar{\sigma}_h$ are tensors of the same form (i.e., with the same vanishing elements and symmetry). This implies that the magnetization

must have the same direction in both components of the material and that this direction coincides with a symmetry axis for both crystal structures with the same symmetry operations. For spherical particles, we can write[10]

$$\Gamma_{\lambda\lambda'} = -\frac{\delta_{\lambda\lambda'}}{3\sigma_e^{\lambda\lambda'}}, \tag{10}$$

where $\delta_{\lambda\lambda'}$ is the Kronecker delta. For highly symmetric conductivity tensors such as in Eq. (1), we can work out Eq. (9) and convert it to a system of only two equations for the two tensor elements σ_e^{xx} and σ_e^{xy} that, for spherical particles, reduce to

$$f\frac{\sigma_p^{xx} - \sigma_e^{xx}}{\sigma_e^{xx} + \frac{1}{3}(\sigma_p^{xx} - \sigma_e^{xx})} + (1-f)\frac{\sigma_h^{xx} - \sigma_e^{xx}}{\sigma_e^{xx} + \frac{1}{3}(\sigma_h^{xx} - \sigma_e^{xx})} = 0, \tag{11}$$

$$f\frac{\sigma_e^{xy} - \sigma_p^{xy}}{\left[\sigma_e^{xx} + \frac{1}{3}(\sigma_p^{xx} - \sigma_e^{xx})\right]^2} + (1-f)\frac{\sigma_e^{xy} - \sigma_h^{xy}}{\left[\sigma_e^{xx} + \frac{1}{3}(\sigma_h^{xx} - \sigma_e^{xx})\right]^2} = 0, \tag{12}$$

where f is the volume fraction of the particles with respect to the total volume (filling factor). Since Eq. (11) contains only the unknown σ_e^{xx}, we can solve it first, and then solve Eq. (12) to obtain σ_e^{xy}. We emphasize that knowledge of the two quantities, σ_e^{xx} and σ_e^{xy}, at all frequencies ω determines unambiguously the response since in the geometry considered (polar magnetization) the term σ_e^{zz} [see Eq. (1)] does not enter the expression for the optical and MO coefficients. Finally, we also remark that Eq. (11) is a quadratic equation with two solutions: one of them does not have a physical meaning and can be discarded[31] since in the limit $f \to 0$ or $f \to 1$, only one solution tends correctly to σ_h^{xx} or σ_p^{xx}.

III. RESULTS

We apply our method to the Mn-Ge alloy system, simulating the MO response in different sample geometries and structures. The final goal is to show how the sample structure affects the MO response and to demonstrate that this method is a powerful tool to understand actual experimental MOKE results, possibly inferring from them the particular sample structure. We consider both cases of diluted Mn in Ge and precipitates of the Mn_5Ge_3 phase in the form of spherical particles.

All our calculations are made in polar geometry and normal incidence (consequently, s and p polarizations coincide), which is the usual reference configuration, since it corresponds to the maximum MO response. In this geometry, the Kerr complex angle for a bulk (semi-infinite) magnetic material is given by[32]

$$\phi_K = \theta_K + i\varepsilon_K = \frac{-\sigma_{xy}}{\sigma_{xx}\sqrt{1 + i\left(\frac{4\pi}{\omega}\sigma_{xx}\right)}}. \tag{13}$$

In the following subsections, we describe systematically the results obtained for different geometries and structures of the Mn-Ge system.

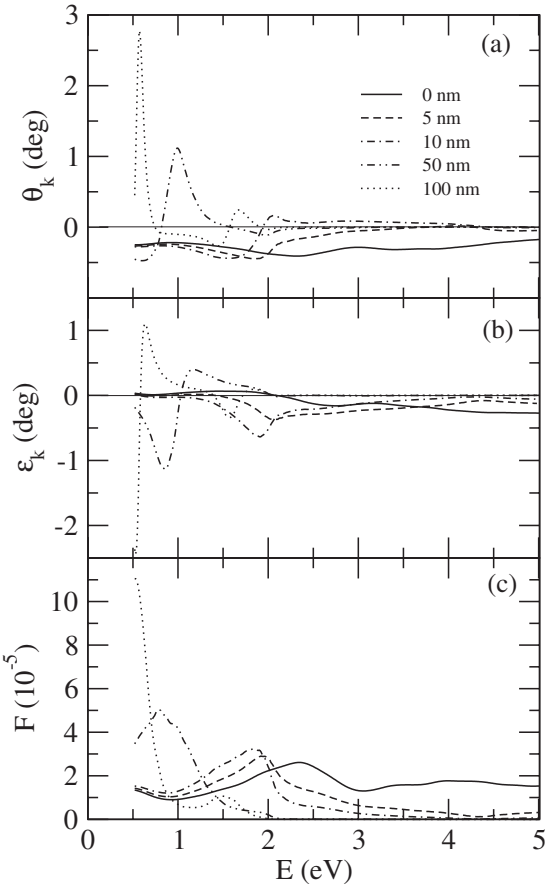

FIG. 1. Polar MOKE spectra at normal incidence of bulk (i.e., semi-infinite medium) Mn_5Ge_3, showing the (a) Kerr angle, (b) ellipticity, and (c) figure of merit [see Eqs. (14) and (15)] as a function of the photon energy for different Ge overlayer thickness.

A. Mn_5Ge_3

Intermetallic Mn_5Ge_3 (Ref. 33) has an hexagonal crystal structure of $D8_8$ type, with experimental cell dimensions at room temperature, a=7.184 Å and c=5.053 Å. The spin state configuration of this compound is likely noncollinear[34] although our simulation assumes a perfect alignment of the magnetic moments, which can be obtained experimentally under a saturating magnetic field.

We remind that the MOKE is strictly linked to the conductivity tensor and, therefore, is calculated on the basis of the band structure,[35,36] taking into account all possible electronic transitions from occupied to unoccupied states [see Eq. (2)]. Therefore, looking at the MOKE spectra, it is possible to identify the interband transitions that contribute to its main features. The spectrum of bulk Mn_5Ge_3 (see Fig. 1, solid line) shows a smooth behavior with a not too pronounced feature at 2.3 eV. Electronic transitions at this energy mainly occur in the minority-spin band while the majority-spin band, being mainly located below the Fermi energy E_F,[27] is expected not to give large contributions (roughly assuming a constant dipole transition matrix). Moreover, transitions mainly occur from states with Mn1-Mn1 character toward Mn1-Mn2 hybridized ones.[27] Since the character of Mn_5Ge_3 is purely metallic, there are many

other possible transitions in all the energy range considered, thus leading to a MOKE spectrum with no prominent peak. A detailed study of the MOKE spectrum of bulk Mn_5Ge_3 is beyond the goal of the present paper and is left to Ref. 37.

Figures 1(a) and 1(b) show the MOKE spectra (rotation and ellipticity, respectively) obtained for "bulk," i.e., semi-infinite Mn_5Ge_3. We also study the effect of capping the magnetic material with a protective nonmagnetic Ge overlayer. We remark that simulations on Mn_5Ge_3 films (not shown) indicate that for thickness above 60 nm the spectra are practically superimposed to the bulk case. This result is due to the highly absorbing (metallic) character of the compound: the radiation, at those film thicknesses, does not reach significantly the Mn_5Ge_3-Ge interface, and the corresponding behavior is merely bulklike.

The spectra of the samples with the nonmagnetic Ge cap present very interesting features. First of all, at significant values of its thickness, a sign change in both rotation and ellipticity occurs, and there is evidence of an oscillating character which is enhanced as the thickness increases. Moreover, the Ge layer introduces a cutoff at an energy which depends on its thickness; as this quantity increases, the absorption coefficient, which is a monotonically growing function above the absorption edge of Ge (~0.7 eV), hinders penetration of the radiation inside the Ge layer until the magnetic material becomes substantially hidden underneath the capping layer. Upon increasing the overlayer thickness, the first maximum of the Kerr rotation shifts toward lower energy and its amplitude is enhanced up to 2.8° at 0.6 eV for a Ge cap of 100 nm. This is an important feature that compared to previous MOKE results on PtMnSb and $MnPt_3$ (Ref. 38) can be defined as Giant Kerr rotation; in fact, its magnitude is much larger than that found up to now for Mn based compounds. In other words, the presence of a capping layer strongly enhances the response, whereas its thickness tunes the energy where the absolute maximum occurs.

In general, in order to definitely state that a Kerr enhancement actually improves the MO performance for possible use in device applications, we need to check the reflectivity behavior at the energy corresponding to the MOKE peak. In fact, the multilayered structure usually induces an oscillating character in energy to the optical response as well. As a consequence, the MO amplification may be completely overwhelmed by a reflectivity reduction since, in that case, the actual detected signal would be weakened. For this kind of evaluation, experimentalists often define a quantity called figure of merit F (see, for example, Ref. 39), which is proportional to the reflectivity and to the second power of the Kerr rotation. Here, we prefer to use a more general definition, which takes into account that all optical and MO parameters are complex quantities,

$$F(\omega) = R(\omega)\phi_k^2(\omega). \tag{14}$$

Here R is the reflectivity of the material, expressed in terms of the reflection coefficients introduced in Sec. II B [see Eqs. (5) and (6)], that is given by $|r_{ss}|^2$ or $|r_{pp}|^2$, for s- or p-polarized incident radiation, respectively; the complex Kerr angle ϕ_k, i.e., ϕ_s or ϕ_p in Eqs. (7) and (8), replaces the mere Kerr rotation θ_k in Ref. 39. It is straightforward to verify that Eq. (14) simply reduces to

$$F = |r_{ps}|^2, \quad \text{or} \quad F = |r_{sp}|^2, \tag{15}$$

for s- or p-polarized incident radiation, respectively.

We calculated this quantity for the uncapped and capped compounds; the results are shown in Fig. 1(c). The general features are confirmed, including the reduction in the signal at high energies (due to the presence of the Ge overlayer) and the oscillating character at low energies (with pronounced maxima whose spacing and position relate to the overlayer thickness). The enhancement of F for the capped material could be exploited, in principle, for optical and MO based devices although we recall that our calculations simulate the Mn_5Ge_3 properties at zero temperature, whereas the Curie temperature of the material is close to room temperature. The physical explanation of a larger MO response can be found in the decreased optical contrast (smaller relative index of refraction) of the interfaces (air-Ge and Ge-Mn_5Ge_3) in the presence of a capping layer with respect to the air-Mn_5Ge_3 interface for the uncapped structure. This phenomenon improves the weight that the magnetic character of the underlying material has on the overall reflected radiation.

Although the figure of merit defined in Eq. (15) is more adequate to describe the true MO response enhancement, reassured by the results of Fig. 1, in the following we prefer to report the Kerr rotation and ellipticity plots since these are more suitable for direct comparison with real experimental results.

B. Mn_xGe_{1-x}

The next step is to calculate the Kerr spectrum of the Mn_xGe_{1-x} system in the hypothesis of perfect dilution, with Mn atoms occupying substitutional lattice sites, as suggested by total energy minimization calculations.[40]

The magneto-optical transitions responsible for the MOKE spectra are again linked to the Mn_xGe_{1-x} band structure: in particular, the main feature at 1.95 eV (2.15 eV) for the $x=0.0625$ (0.125) Mn concentration can be associated to transitions involving the t_{2g} dangling-bond hybrid (DBH) and the e_g and t_{2g} crystal-field resonances (CFR) above E_F.[41,42] The same feature is also found in the diagonal (optical) and off-diagonal (magneto-optical) conductivity tensor elements.[37] The Mn-concentration dependence seen comparing the two cases can be related to changes in the band structure (mainly due to band-folding effects[37]) rather than to differences in the nature of the MOKE interband transitions.

In order to achieve high magnetic ordering temperature, the structure must contain enough dopant atoms (typically a concentration of a few percent), a situation that in principle is achievable by standard epitaxial growth methods, such as low-temperature MBE techniques, although rather difficult in practice.[43] From the computational point of view, we will describe the MO properties of this material as a function of the sample composition and geometry; we will also consider alternative structures that might originate in the Mn-Ge system growth, such as precipitation of Mn_5Ge_3 nanoparticles.

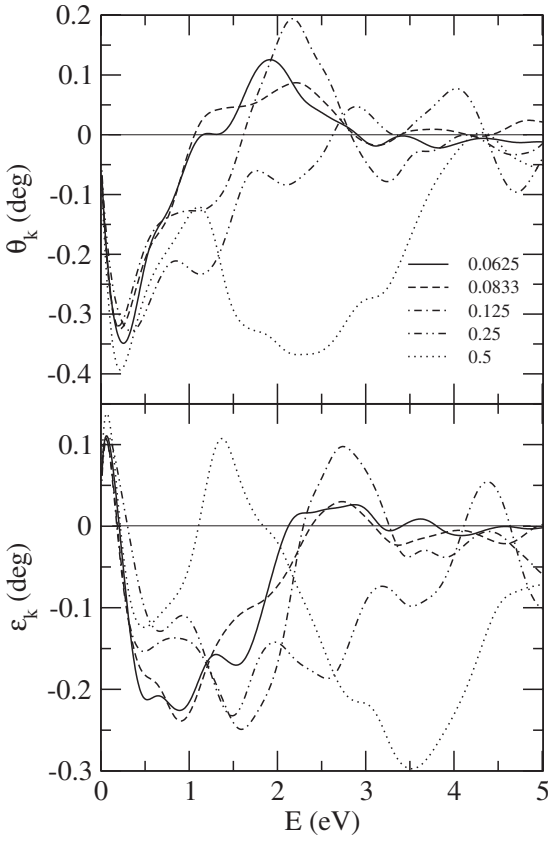

FIG. 2. Polar MOKE spectra of bulk Mn_xGe_{1-x} as a function of the Mn concentration, x.

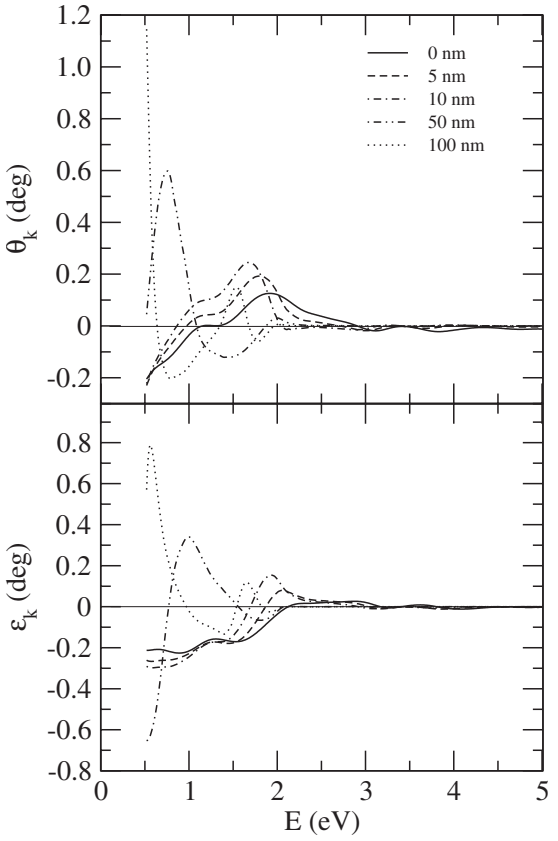

FIG. 3. Polar MOKE spectra of bulk $Mn_{0.0625}Ge_{0.9375}$ as a function of Ge capping layer thickness.

First of all, we are interested in observing the effect of the dopant concentration on the MO properties of DMS. We have considered several Mn dilutions from $x=0.0625$ to 0.5. In those simulations, we used the pure Ge lattice constant (5.65 Å) since energy minimization calculations indicate that no appreciable variation in the unit-cell parameter occurs when Ge is substituted by Mn.[40]

The bulk MOKE spectra are reported in Fig. 2. We remark that, of course, the largest concentrations, 25% and 50%, are not experimentally achievable in diluted form. However, they are useful for our purposes since they show that the spectra are not merely linearly dependent on concentration: this evidence sets a limit to the use of concentration as a tuning parameter for MO response optimization. Both rotation and ellipticity present several peaks and features which are consequences of the spin-resolved electronic structure. As in the Mn_5Ge_3 system due to the presence of dopants, the optical absorbing character of the material causes the spectra to remain almost unchanged if, instead of bulk DMS, films down to about 150 nm thick are considered (not shown).

Since only low concentrations have been experimentally achieved so far, we selected the 6.25% DMS phase, which is very close to typically reported experimental values,[2–4,44,45] for additional analysis. Figure 3 shows the MOKE spectra at this Mn concentration, comparing the result for the uncapped and capped bulk material. The overlayer affects the spectra similarly to that found for the Mn_5Ge_3 case; here, the peaks of the spectrum are centered at slightly lower energies. However, the tuning effect of the capping layer thickness on the MO spectrum is still present. Therefore, nonmagnetic capping layers are confirmed to enhance the MO response and, at the same time, to tune the wavelength corresponding to the maximum of the MO signal.

C. Mn_5Ge_3 nanograins in Ge

We now investigate the effect of Mn_5Ge_3 nanoparticles dispersed into the Ge matrix. As mentioned before, this situation occurs very often during the growth of Mn-Ge compounds,[5] and we want to ascertain how this influences the MO response. We assume that the mean size of the grains is much smaller than the wavelength of the probing radiation. This is a reasonable assumption since, for example, experimental measurements on Mn-ion implanted Ge samples report Mn_5Ge_3 particle size of the order of 10 nm,[5] whereas in our simulations the minimum wavelength considered is 248 nm. Under these conditions, we can use the EMA to calculate the σ tensor of the effective medium composed of matrix and particles, using the individual tensors of the host Ge and Mn_5Ge_3 particles. Clearly, we also assume that the latter system maintains the properties of the bulk material; i.e., we neglect surface and size effects.

Before proceeding with the simulations, we must ascertain whether the conductivity tensor of the particles and the matrix have the same form. In fact, magnetic hysteresis loops for high-quality single phase $Mn_5Ge_3(0001)$ films grown via solid-phase epitaxy on Ge(111) and GaAs(111) demonstrate

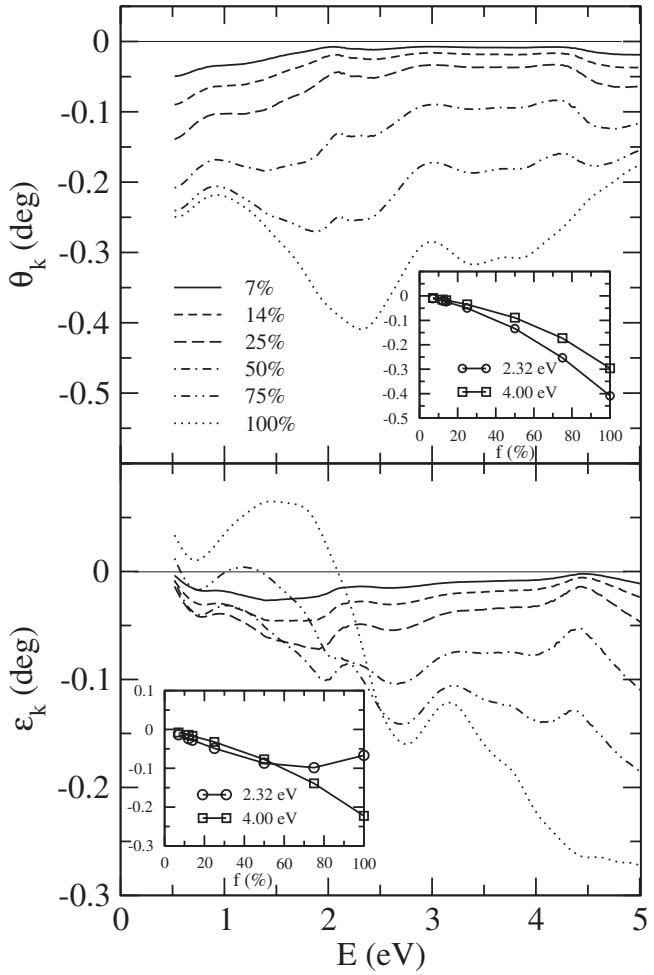

FIG. 4. Polar MOKE spectra of Mn_5Ge_3 spherical particles in a Ge matrix (bulk case) as a function of particle volume fraction, using the effective-medium approximation. The insets show the trend of θ_k (upper panel) and ε_k (lower panel) as a function of the filling factor f at fixed wavelength. A linear dependence is observed for small values of f.

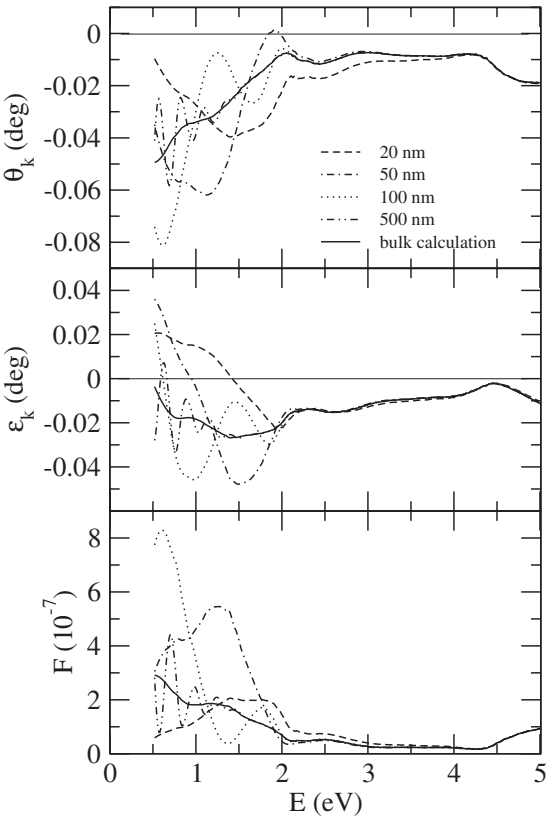

FIG. 5. EMA polar MOKE spectra and figure of merit (bottom panel) of 7% Mn_5Ge_3 in a Ge matrix as a function of film thickness.

that the easy axis of the film lies in plane due to shape anisotropy.[46] In-plane magnetization would make our calculations more cumbersome since it would result in a σ tensor of Mn_5Ge_3 that is not antisymmetric as the σ tensor of the Ge matrix, and the determination of the effective conductivity tensor would be much more complex than the one leading to Eqs. (11) and (12). However, we can make use of the experimental evidence on Mn_5Ge_3 clusters in Ge(001)[5,9] showing that the nanoparticles grow with their [0001] axis parallel to the [001] Ge crystal-axis: this makes it reasonable for us to assume polar geometry in our simulation since the [0001] axis constitutes an uniaxial easy magnetization direction for crystal anisotropy. Therefore, the desired symmetry of the conductivity tensor is assured.

In Fig. 4, we show the calculated MOKE spectra in the framework of EMA, for Mn_5Ge_3 spherical particles in a pure Ge matrix, with a uniform dispersion of the clusters inside the matrix corresponding to several filling factors, f. We observe at low concentration an initial linear dependence of both rotation and ellipticity as a function of Mn content. This is evidenced in the insets where we plot the MOKE as a function of f at fixed wavelength. At larger f values, before recovering the response of pure Mn_5Ge_3, there is a departure from this linearity. This is particularly evident in the ellipticity spectrum.

We emphasize that some qualitative features of the pure Mn_5Ge_3 response are preserved even at very low filling factors since the general structure of the spectrum and the position of maxima and minima are maintained. This constitutes an important result in view of the possibility to infer from MOKE measurements the presence of Mn_5Ge_3 precipitates in the structure of binary Mn-Ge compounds. On the contrary, as discussed in the previous section, the shape of the spectra for the DMS phase (Fig. 2) is much more dependent on the Mn dilution.

We further investigated the nanogranular system with a particle filling factor equal to 7%, comparable to the values obtained in experiments, as mentioned previously. Figure 5 shows the MOKE spectra obtained within EMA and the relative figure of merit for films constituted by spherical Mn_5Ge_3 particles in Ge at various film thicknesses. Here, and in all following cases in which we treat film structures, the final (substrate) material is germanium.

At variance with the systems described in the previous subsections, there is a clear difference with respect to the bulk calculation even at considerably large thickness. This is due to the dominant features of the semiconducting Ge, which assures that the effective medium maintains its transparency for a large portion of the spectrum. At high energy,

the various spectra tend to overlap as the incident beam does not reach the second interface and the behavior of the film becomes bulklike. This limit starts at the energy where the penetration depth is equal to the thickness of the film. At low energy, the thickness of the magnetic effective medium itself exhibits filter-amplifier character, introducing oscillating features in the spectrum and a selective enhancement of the MO response. This behavior has a different origin with respect to the analogous result observed in the presence of a capping layer (see discussion in Sec. III A). In the present case, the finite thickness of the magnetic film enhances the real MOKE response, as proven by the figure of merit spectrum, since a significant contribution to the overall reflected radiation comes from the fraction which crosses the magnetic layer and is reflected back accumulating a MO variation in polarization proportional to the thickness. Obviously, if the magnetic layer becomes too thick, its absorption character becomes overwhelming, canceling such a contribution. In this way, we can infer that there must exist an intermediate thickness such that the amplitude is maximum at a given radiation energy.

The addition of a capping layer to such film structures (not shown) introduces further modulation to the spectra; the signal amplitude grows with a significant enhancement of the oscillating character at low energies and with a reduction in the cutoff energy which may be below 2 eV for even larger thickness. This extends the conclusions already drawn concerning the effect of nonmagnetic layers on the MO response to all the materials.

D. Mn_5Ge_3 inhomogeneous distribution profile

The next step is to improve our model in order to simulate samples with nonuniform MO active constituents since this may constitute an additional contribution to MOKE engineered design. In the previous sections, we studied in detail the effect of the sample structure, considering an homogeneous Mn distribution over the entire sample thickness. However, this may not be true for most real samples so we extend our model to simulate nonuniform profiles as well. We concentrate on films of intermediate thickness, which are those typically found in the literature, since they are easily obtained by usual growth techniques, such as MBE, or other fabrication methods, such as ion implantation. We emphasize that ultrathin films may not be well simulated by our calculations since in that limit the materials may lose their bulk properties, acquiring anomalous structural and magnetic features linked to reduced dimensionality effects. We choose, as an example, a typical thickness of 150 nm, keeping in mind that different values do not give qualitatively different results but only variations on details of the spectra modulation.

As a simple attempt, we account for the inhomogeneous distribution of Mn considering a system made of two layers, each 75 nm thick, with Mn_5Ge_3 clusters in a Ge matrix corresponding to $f=9.0\%$ and 5.0%, respectively. In this way, the average filling factor is kept at 7%. Both possibilities are considered: if the Mn-rich layer is on top, we have what we call "decreasing concentration profile;" if the opposite case occurs, the resulting bilayer is defined as having an "increasing concentration profile." We show in Fig. 6 the results obtained. In these spectra, we distinguish two energy intervals: the region for $E \geq 2$ eV, which we may consider bulklike, shows essentially the properties due to the first layer exposed to the radiation and, therefore, resembles the results already shown in the high-energy part of the spectra of Fig. 4; the interval for $E < 2$ eV is dominated by the geometrical (thickness) parameter of the film. We emphasize that the position of the minima and maxima for the curves (both rotation and ellipticity) is almost the same, independent of the concentration profile. This means that the significant parameter (compare with Fig. 5) is the overall thickness of the magnetic film (150 nm in our case). Remarkably, the specific profile affects only the magnitude of the peaks. We observe that the modulation of the spectra is larger for the increasing concentration profile and smaller for the decreasing concentration profile. This trend follows the previous discussion regarding the capping layer: radiation reflected by more internal interfaces is more effective when the optical contrast between the materials above is minimized. In our case, this occurs for the increasing concentration, which represents the situation where the interference effect is more evident.

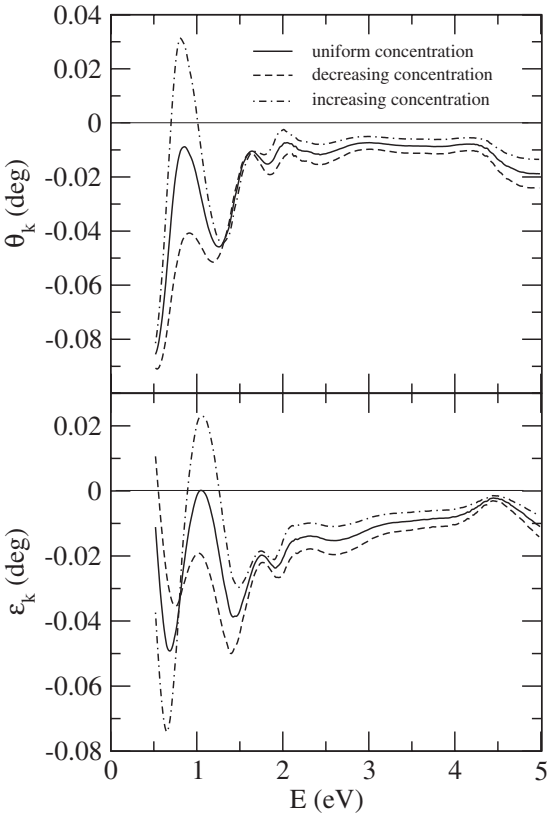

FIG. 6. EMA polar MOKE spectra of Mn_5Ge_3 particles in a Ge matrix with a uniform (7%) and nonuniform Mn_5Ge_3 concentration profile. In all cases the total film thickness is 150 nm; the nonuniform concentration profile samples are made of two layers, each 75 nm thick, with particle volume fraction equal to 5% and 9%, respectively: the decreasing (increasing) concentration profile sample has the topmost layer corresponding to the higher (lower) particle volume fraction.

Another interesting possible tuning of the MO response is related to the effect of a nonmagnetic layer inside a multi-

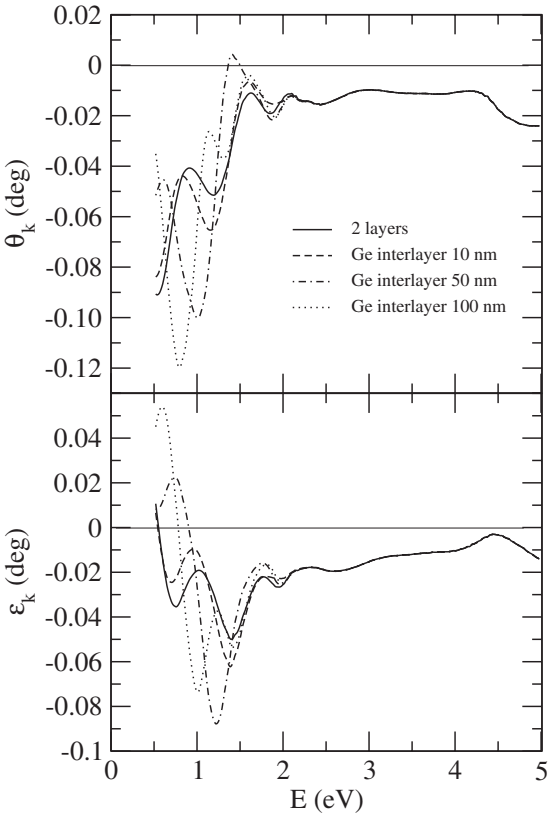

FIG. 7. EMA Polar MOKE spectra of a trilayer containing Mn_5Ge_3 particles in a Ge matrix as a function of the Ge interlayer thickness. The topmost 75-nm-thick layer (with particle filling fraction equal to 9%) is followed by a pure Ge interlayer and then by a 75-nm-thick layer with particle filling fraction equal to 5%. Different curves refer to different values of the interlayer thickness.

layered structure. For example, we can place such a layer between two magnetic layers to obtain the sequence magnetic/nonmagnetic/magnetic layers. In our simulation, we consider a system consisting of two 75-nm-thick effective media of Mn_5Ge_3 spherical particles in Ge separated by a layer of pure Ge and placed on a Ge semi-infinite substrate. The two magnetic layers are chosen assuming filling factors equal to 9% and 5%, respectively, as in the decreasing concentration profile previously described, with the larger particle concentration in the topmost layer. The MO spectra, for different values of the interlayer thickness, are shown in Fig. 7. Obviously, the presence of the interlayer changes the spectra only at an energy below 2 eV: above this energy, the spectra are all superimposed since the penetration depth is lower than the thickness of the first magnetic layer, as previously discussed. At lower energies, where the Ge interlayer contributes to the response, we find an amplification and modulation effect similar to that described for the capping layer in Sec. III A (Fig. 1): the Kerr rotation and ellipticity spectra present sharp and definite peaks, whose amplitudes increase with the interlayer thickness, while their positions shift toward lower energies. For example, for the larger interlayer thickness reported in Fig. 7, the absolute value of the Kerr rotation is 0.12° at about 0.8 eV, whereas the ellipticity is 0.09° at 1.2 eV. In principle, this can be a useful feature to exploit for device applications.

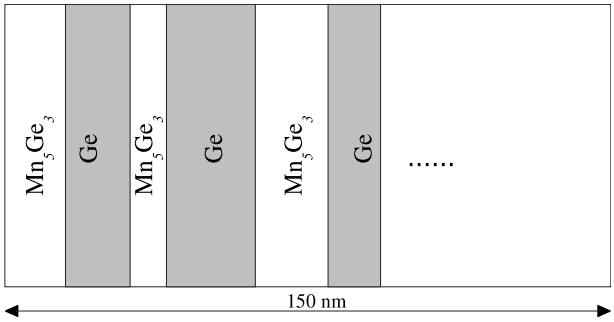

FIG. 8. Alternating composition layers model scheme. The multilayer is used to simulate the nanogranular structure of the two intermixed phases.

E. Alternating composition layers approximation

We can extend our modeling even further and build up structures to increase the possibility of tuning the MO response. What would happen if we make up a system of many thin magnetic layers intercalated by layers made of a nonmagnetic material? Would this structure, in the limit of a large number of alternating magnetic/nonmagnetic thin layers, coincide with a continuous medium constituting of magnetic inclusions homogeneously dispersed in a nonmagnetic medium? If this were the case, this construction could be used to simulate an arbitrary profile of nanoparticle concentration dispersed in a matrix. In order to answer these questions, we approximate our sample by building up a stack consisting of thin Mn_5Ge_3 layers separated by Ge layers (see Fig. 8). With this so-called alternating composition layers approximation (ACLA), we consider the multilayer as a sequence of several Mn_5Ge_3-Ge bilayers: at this point, the correct Mn concentration is assured adjusting the relative thickness of the two layers constituting each bilayer, and we study the MO response as a function of the number and thickness of the layers.

For example, if we want to approximate the uniform Mn distribution (7% particle filling factor, the reference value used above) of a 150-nm-thick film with two Mn_5Ge_3-Ge pairs, we have to consider films of Mn_5Ge_3 and Ge with thickness 5.25 and 69.75 nm, respectively. Then, we can refine the approximation by increasing the number of pairs while decreasing accordingly the thickness of each film so as to preserve the overall thickness of the stack. The resulting spectra are shown in Fig. 9. We arbitrarily decided to start each pair with the Mn_5Ge_3 layer on top, a choice that, of course, affects the calculated spectra for a small number (high thickness) of the pairs, but that becomes irrelevant in the opposite limit. As shown in Fig. 9, as the number of pairs increases, the ACLA MOKE spectra tend to converge to the continuum limit, i.e., when the thickness of each layer becomes negligible with respect to the wavelength of the radiation, and accordingly the number of layers tends to infinity.

We checked the convergence degree of the ACLA MOKE spectrum by observing the absolute value of the Kerr rotation as a function of the number of pairs considered at fixed energy values. As an example, in the inset to Fig. 9, we report the results at 2.5 eV, a value corresponding to a peak with a structural character (not affected by the geometrical oscilla-

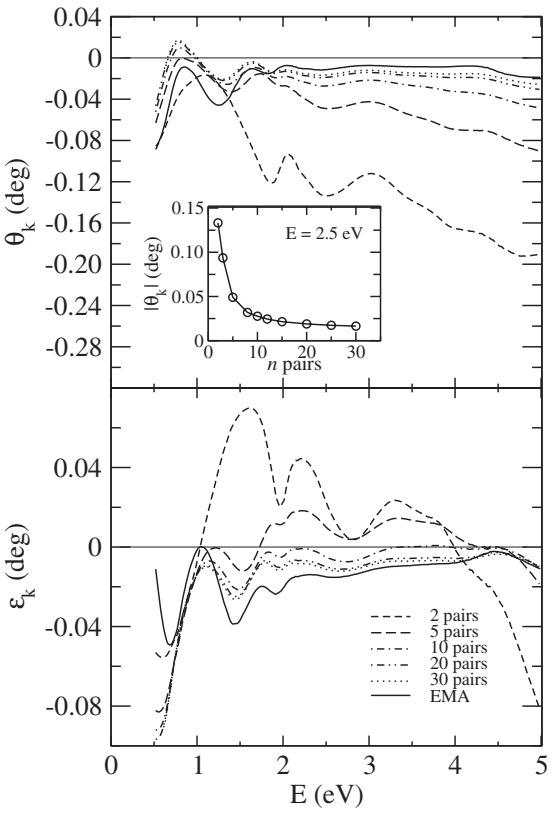

FIG. 9. ACLA Polar MOKE spectra as a function of the number of Mn_5Ge_3/Ge layer pairs. The Mn_5Ge_3 volume fraction is 7%, and the total sample thickness is kept constant (150 nm). The EMA spectrum (solid line) is also reported for comparison. The inset shows the trend of the ACLA Kerr rotation (absolute value) at 2.5 eV as a function of Mn_5Ge_3/Ge layer pairs number.

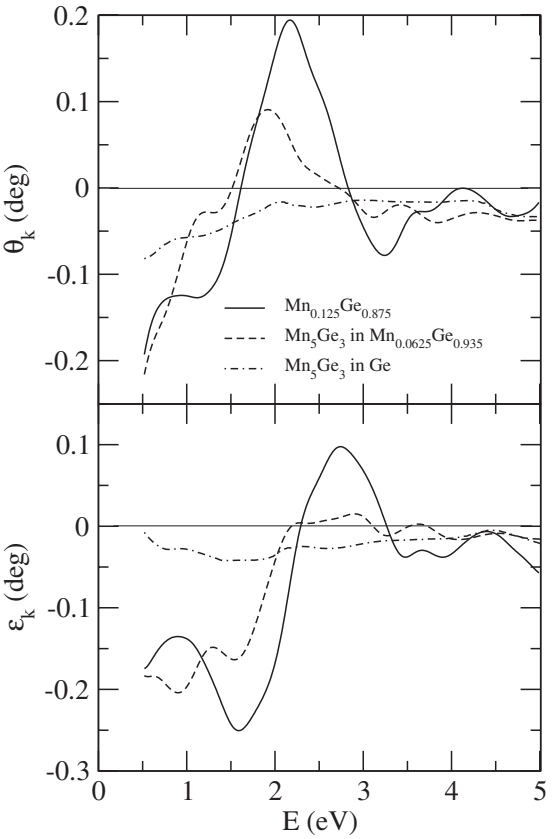

FIG. 10. Polar MOKE spectra of bulk Mn-Ge. Three different compositions are compared: (i) $Mn_{0.125}Ge_{0.875}$ DMS, (ii) Mn_5Ge_3 particles in a $Mn_{0.0625}Ge_{0.9375}$ DMS matrix, and iii) Mn_5Ge_3 particles in a pure Ge matrix. In the second and third cases, the particle filling factor is adjusted in order to keep a total Mn concentration equal to 12.5%, the same as the first case.

tory behavior observed in the lower portion of the energy spectrum). Comparing the converged spectrum with the single layer EMA spectrum, we can see that they are not identical although the general features are similar, with peaks at the same energy positions. We attribute these differences to the distinct geometrical characteristic of the magnetic inclusions. In particular, the spherical geometry of the clusters considered in the EMA and the layered structure in the ACLA imply different demagnetizing factors, which may account for the discrepancy in the spectra.

F. Mn_5Ge_3 grains in $Mn_{0.0625}Ge_{0.9375}$

A relevant issue to address at this point is to ascertain how the presence of both diluted Mn and magnetic precipitates affects the MO response. This is a very important question since most experiments suggest that, in the attempt of growing DMS, a portion of the magnetic species produces precipitates. Therefore, the diluted phase often coexists with a precipitate magnetic phase in the same sample. To this end, we make use of the EMA approach once again: we replace the Ge host with a DMS $Mn_{0.0625}Ge_{0.9375}$ matrix, where Mn atoms occupy substitutional lattice sites of the Ge crystal, as in Sec. III D, and we consider Mn_5Ge_3 particles with a filling factor corresponding to 6.25% Mn concentration. The MO calculations were made with the same procedure used in previous sections. In Fig. 10, we show the MOKE calculations for the above mentioned system and compare it with two others: (i) bulk $Mn_{0.125}Ge_{0.875}$ and (ii) Mn_5Ge_3 particles in a pure Ge host with a filling factor corresponding to 12.5% Mn concentration. In this way, we compare the MOKE spectra for three samples with the same total Mn content. We observe that the MOKE response is very sensitive to the microscopic compositional character of the sample. The features of the two samples containing DMS are similar: the details in the peak positions and amplitudes depend on the amount of precipitated Mn, but the overall behavior is comparable. On the contrary, when Mn is present only in the nanoparticles (third sample), the MO response is much lower and much less structured. Therefore, the spectra can be used to obtain a signature of the existence of a DMS structure.

G. Changing the magnetic material: Fe in Ge

Although we focused attention on the Mn-Ge system, our methodology can be applied to any choice of magnetic/nonmagnetic material. Actually, in order to optimize engineered structures, an important objective is to understand the relevance of the particular magnetic material chosen for a

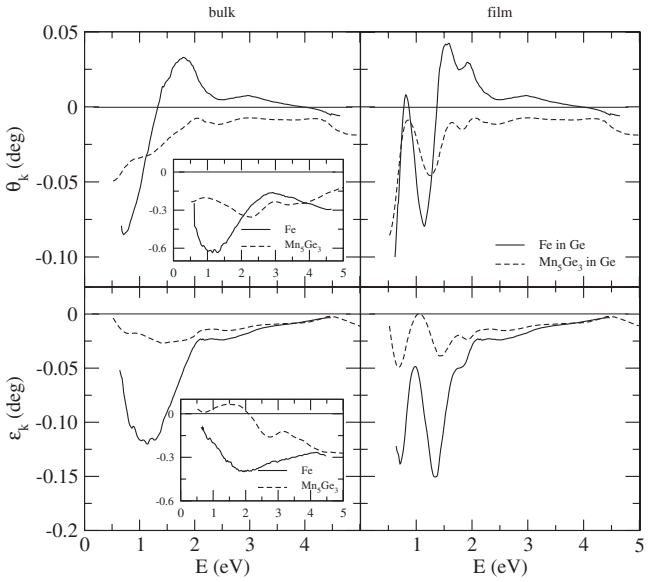

FIG. 11. Comparison between the polar MOKE spectra of Fe nanoparticles and Mn_5Ge_3 particles in a Ge matrix. Left panels show the bulk calculations, whereas right panels report 150-nm-thick film calculations. The inset in the left panels shows the comparison between the pure bulk Fe and pure bulk Mn_5Ge_3.

given geometry and sequence of the multilayered structure. Moreover, it is interesting to understand how much the main features of the MO spectra are merely due to the particular geometry of the sample (thickness, capping, volume fraction of magnetic precipitates, etc.) rather than to the structural and magnetic properties of the specific material. For this reason, as an example, we replace Mn_5Ge_3 particles with Fe particles in the Ge matrix. Since iron has a cubic structure, its σ tensor fulfills the requirements of our theoretical approach (see Sec. II C).

The conductivity tensor for Fe was derived with our *ab initio* procedure and tested comparing the calculated bulk MOKE spectrum with experimental data:[26,47] the results are in satisfactory agreement. As in previous calculations, we consider spherical Fe particles in a nonmagnetic Ge matrix in the EMA approximation. The results obtained for the EMA-MOKE calculations at 7% Fe filling factor are reported in Fig. 11 for bulk and a 150-nm-thick film and are compared with analogous simulations for the Mn_5Ge_3 in Ge. As we can see, the order of magnitude of the spectra is the same and the main features of the film curves (peak positions) are the same. The latter effect is due exclusively to the sample structure, i.e., film thickness. As a result of the higher MOKE signal in iron with respect to Mn_5Ge_3 (see insets of Fig. 11), the presence of different magnetic inclusions in the host matrix implies changes in the amplitude of the spectra. While the geometrical structure of the sample dictates the shape of the MOKE spectra, these findings show that the nature of the magnetic material affects the magnitude of the spectra.

IV. CONCLUSIONS

We systematically studied the MO response of the Mn-Ge binary system. MOKE spectra for different geometrical sample structures, in the presence of perfect dilution of Mn in Ge, precipitation of the magnetically relevant Mn_5Ge_3 phase, and intermixing of the two phases, were considered and analyzed in detail. The problem of an inhomogeneous composition was approached following two approximations: (i) assuming a distribution of spherical magnetic inclusions in a nonmagnetic matrix (EMA) and (ii) considering an alternating arrangement of magnetic/nonmagnetic thin layers (ACLA). We showed that besides the choice of the particular magnetic species and the host matrix the MOKE response can be tuned, controlling several parameters such as the magnetic layer thickness, magnetic species concentration (average value and specific profile), and thickness of possible nonmagnetic overlayer or interlayer. This potentially allows the prediction and design, using *ab initio* calculations, of suitably engineered structures for MO device applications. Moreover, systematic simulations of different arrangements of composite systems and their comparison with experimental results may constitute a basis to use MOKE spectra as fingerprints of the structural, magnetic, and geometrical properties of the system, thus contributing to obtaining a full characterization of magnetic materials.

ACKNOWLEDGMENTS

We gratefully acknowledge Silvia Picozzi for useful discussions. Work at Northwestern University was supported by the U.S. NSF (through its MRSEC program at the N. U. Materials Research Center).

[1] J. A. Gaj, J. Ginter, and R. R. Galazka, Phys. Status Solidi B **89**, 655 (1978).
[2] Y. D. Park, A. T. Hanbicki, S. C. Erwin, C. S. Hellberg, J. M. Sullivan, J. E. Mattson, T. F. Ambrose, A. Wilson, G. Spanos, and B. T. Jonker, Science **295**, 651 (2002).
[3] A. P. Li, J. Shen, J. R. Thompson, and H. H. Weitering, Appl. Phys. Lett. **86**, 152507 (2005).
[4] L. Ottaviano, M. Passacantando, S. Picozzi, A. Continenza, R. Gunnella, A. Verna, G. Bihlmayer, G. Impellizzeri, and F. Priolo, Appl. Phys. Lett. **88**, 061907 (2006).
[5] M. Passacantando, L. Ottaviano, F. D'Orazio, F. Lucari, M. De Biase, G. Impellizzeri, and F. Priolo, Phys. Rev. B **73**, 195207 (2006).
[6] A. Verna, L. Ottaviano, M. Passacantando, S. Santucci, P. Picozzi, F. D'Orazio, F. Lucari, M. De Biase, R. Gunnella, M. Berti, A. Gasparotto, G. Impellizzeri, and F. Priolo, Phys. Rev. B **74**, 085204 (2006).
[7] L. Ottaviano, M. Passacantando, A. Verna, R. Gunnella, E. Principi, A. Di Cicco, G. Impellizzeri, and F. Priolo, J. Appl. Phys. **100**, 063528 (2006).

[8] A. Verna, F. D'Orazio, L. Ottaviano, M. Passacantando, F. Lucari, G. Impellizzeri, and F. Priolo, Phys. Status Solidi A **204**, 145 (2007).
[9] C. Bihler, C. Jaeger, T. Vallaitis, M. Gjukic, M. S. Brandt, E. Pippel, J. Woltersdorf, and U. Gösele, Appl. Phys. Lett. **88**, 112506 (2006).
[10] D. Stroud, Phys. Rev. B **12**, 3368 (1975).
[11] J. Zak, E. R. Moog, C. Liu, and S. D. Bader, J. Magn. Magn. Mater. **89**, 107 (1990).
[12] J. Zak, E. R. Moog, C. Liu, and S. D. Bader, Phys. Rev. B **43**, 6423 (1991).
[13] J. L. Dormann, D. Fiorani, and E. Tronc, Adv. Chem. Phys. **98**, 283 (1997).
[14] J. L. Dormann, D. Fiorani, F. Giammaria, and F. Lucari, J. Appl. Phys. **69**, 5130 (1991).
[15] I. D. Borcia, P. Beauvillain, B. Bertenlian, P. Gogol, and R. Mégy, J. Magn. Magn. Mater. **301**, 258 (2006).
[16] C. Clavero, A. Cebollada, G. Armelles, Y. Huttel, J. Arbiol, F. Peirò, and A. Cornet, Phys. Rev. B **72**, 024441 (2005).
[17] J. L. Menéndez, B. Bescós, G. Armelles, R. Serna, J. Gonzalo, R. Doole, A. K. Petford-Long, and M. I. Alonso, Phys. Rev. B **65**, 205413 (2002).
[18] J. S. Ahn, K. H. Kim, T. W. Noh, Doh-Hyung Riu, Kyung-Ho Boo, and Hyoun-Ee Kim, Phys. Rev. B **52**, 15244 (1995).
[19] M. V. Vashuk, E. A. Gan'shina, S. Phonghirun, I. I. Tulsky, P. N. Sherbak, and Y. E. Kalinin, J. Non-Cryst. Solids **353**, 962 (2007).
[20] V. M. Maevsky, Phys. Met. Metallogr. **59**, 213 (1985).
[21] K. H. J. Buschow, in *Ferromagnetic Materials*, edited by E. P. Wohlfarth and K. H. J. Buschow (North-Holland, Amsterdam, 1988), Vol. 4, p. 493.
[22] C. S. Wang and J. Callaway, Phys. Rev. B **9**, 4897 (1974).
[23] H. Ebert, Rep. Prog. Phys. **59**, 1665 (1996).
[24] E. Wimmer, H. Krakauer, M. Weinert, and A. J. Freeman, Phys. Rev. B **24**, 864 (1981).
[25] H. Monkhorst and J. D. Pack, Phys. Rev. B **13**, 5188 (1976).
[26] F. Ricci, M.S. thesis, Università di L'Aquila, 2006.
[27] S. Picozzi, A. Continenza, and A. J. Freeman, Phys. Rev. B **70**, 235205 (2004).
[28] S. Picozzi, A. Continenza, M. Kim, and A. J. Freeman, Phys. Rev. B **73**, 235207 (2006).
[29] H. R. Philipp and E. A. Taff, Phys. Rev. **113**, 1002 (1959).
[30] J. A. Osborn, Phys. Rev. **67**, 351 (1945).
[31] D. Stroud, Superlattices Microstruct. **23**, 567 (1998).
[32] W. Reim, J. Magn. Magn. Mater. **58**, 1 (1986).
[33] J. B. Forsyth and P. J. Brown, J. Phys.: Condens. Matter **2**, 2713 (1990).
[34] A. Stroppa and M. Peressi, Phys. Status Solidi A **204**, 44 (2007).
[35] A. Stroppa, S. Picozzi, A. Continenza, M. Y. Kim, and A. J. Freeman, Phys. Rev. B **77**, 035208 (2008).
[36] F. Ricci, S. Picozzi, A. Continenza, F. D'Orazio, F. Lucari, K. Westerholt, M. Kim, and A. J. Freeman, Phys. Rev. B **76**, 014425 (2007).
[37] F. Ricci, F. D'Orazio, A. Continenza, F. Lucari, and A. J. Freeman (unpublished).
[38] P. M. Oppeneer, V. N. Antonov, T. Kraft, H. Eschrig, A. N. Yaresko, and A. Ya. Perlov, Solid State Commun. **94**, 255 (1995).
[39] T. Yoshino and S. Tanaka, Jpn. J. Appl. Phys. **5**, 989 (1966).
[40] A. Continenza, G. Profeta, and S. Picozzi, Phys. Rev. B **73**, 035212 (2006).
[41] P. Mahadevan and A. Zunger, Phys. Rev. B **69**, 115211 (2004).
[42] A. Stroppa, S. Picozzi, A. Continenza, and A. J. Freeman, Phys. Rev. B **68**, 155203 (2003).
[43] K. M. Yu, W. Walukiewicz, T. Wojtowicz, I. Kuryliszyn, X. Liu, Y. Sasaki, and J. K. Furdyna, Phys. Rev. B **65**, 201303(R) (2002).
[44] L. Ottaviano, M. Passacantando, S. Picozzi, A. Continenza, R. Gunnella, G. Bihlmayer, G. Impellizzeri, and F. Priolo, Appl. Phys. Lett. **88**, 061907 (2006).
[45] P. De Padova, J.-P. Ayoub, I. Berbezier, P. Perfetti, C. Quaresima, A. M. Testa, D. Fiorani, B. Olivieri, J.-M. Mariot, A. Taleb-Ibrahimi, M. C. Richter, O. Heckmann, and K. Hricovini, Phys. Rev. B **77**, 045203 (2008).
[46] See, for example, R. Gunnella, L. Morresi, N. Pinto, R. Murri, L. Ottaviano, M. Passacantando, F. D'Orazio, and F. Lucari, Surf. Sci. **577**, 22 (2005), and Ref. 19 therein.
[47] A. Delin, O. Eriksson, B. Johansson, S. Auluck, and J. M. Wills, Phys. Rev. B **60**, 14105 (1999).